Journal of Nonlinear Modeling and Analysis
Volume 4, Number 3, September 2022, 539–561
http://jnma.ca; http://jnma.ijournal.cn
DOI:10.12150/jnma.2022.539

Spatiotemporal Dynamic Analysis in a Time-space Discrete Brusselator Model

Hongxia Liu[1], Ranchao Wu[1,†] and Biao Liu[2]

Abstract In this paper, we study the spatiotemporal patterns of a Brusselator model with discrete time-space by using the coupled mapping lattice (CML) model. The existence and stability conditions of the equilibrium point are obtained by using linear stability analysis. Then, applying the center manifold reduction theorem and the bifurcation theory, the parametric conditions of the flip and the Neimark-Sacker bifurcation are described respectively. Under space diffusion, the model admits the Turing instability at stable homogeneous solutions under some certain conditions. Two nonlinear mechanisms, including flip-Turing instability and Neimark-Sacker-Turing instability, are presented. Through numerical simulation, periodic windows, invariant circles, chaotic phenomenon and some interesting spatial patterns are found.

Keywords Discrete Brusselator model, Bifurcation, Turing instability, Couple map lattice.

MSC(2010) 34C23, 37G10, 39A28.

1. Introduction

In 1952, Turing [29] proposed the reaction-diffusion coupling equation for the first time, and obtained that the system transforms from a stable process to an unstable process under the action of diffusion. He believed that the diffusion may destroy the spatial homogeneous states and lead to non-homogeneous spatial patterns. This instability is known as the Turing instability, which has been also known as the diffusion-driven instability. In recent decades, Turing instability has been applied to many fields such as biology, physics, chemistry, etc. In chemical systems, Turing patterns can be produced by a number of reactions such as the famous Brusselator model.

Brusselator model, as an autocatalytic reaction, was proposed by Prigogine and Lefever [23] in the 1960s. Since then, it has attracted the attention of many scholars, and detailed theoretical analysis and experimental research have been carried out on the dynamic behavior of Brusselator system in continuous time and space. It has been found that Hopf bifurcation and Turing instability would occur in the continuous Brusselator system. The combination of Hopf bifurcation and Turing

[†]the corresponding author.
Email address: rcwu@ahu.edu.cn (R. Wu), lhxdwl23@163.com (H. Liu), liubiao0807@126.com (B. Liu)
[1]School of Mathematics Science, Anhui University, Hefei, Anhui 230601, China
[2]School of Mathematics and Physics, Anhui Jianzhu University, Hefei, Anhui 230601, China
*The authors were supported by National Natural Science Foundation of China (Nos. 11971032, 62073114).

instability can produce some patterns. For example, it refers to [7, 9, 11, 15, 16, 18] and their relevant literature.

In many cases, however, it is not continuous in time. For example, in [25], the nonlinear dynamical behaviors of two discrete-time versions of the continuous time Brusselator model were considered. Moreover, in [6], the dynamics of Brusselator model with discrete time were studied, and a new chaos control method was proposed based on bifurcation theory and center manifold theorem to control the chaos of Brusselator model with discrete time under the influence of flip and Hopf bifurcation.

As we know, there are many methods that can establish the discrete model. Since the coupled mapping lattice (CML) model can discretize the corresponding continuous reaction diffusion model, it has been widely used (see [3,13,28,31,33–35]). The continuous system is discretized by CML model, which leads to the unique nonlinear mechanism and characteristics of the time-space discrete Brusselator system. The most important nonlinear mechanisms are the various bifurcation behaviors, including flip bifurcation and Neimark-Sacker bifurcation. As a unique bifurcation phenomenon of discrete Brusselator system, flip bifurcation can lead to the formation of the path to chaos accompanied by period-doubling process. The combination of flip bifurcation and Turing instability can lead to the formation of complex pattern patterns. As described in [17], Neimark-Sacker bifurcation in the discrete system is the discrete counterpart of the Hopf bifurcation that occurs in the continuous system. The combination of Neimark-Sacker bifurcation and Turing instability gives rise to Neimark-Sacker-Turing instability, resulting in periodic orbits, invariant circles, chaotic attractors and other complex patterns, which are of exploratory significance. Therefore, we will consider the dynamical behavior of the time-space discrete Brusselator model in this paper.

The center manifold reduction and normal form theory are frequently used in the study of the bifurcation. For example, in [12], the stability and local Hopf bifurcation of Leslie-Gower predator-prey system with discrete distributed delay were studied. By using the center manifold reduction and normal form theory, formulas were obtained to determine the stability and direction of periodic solutions of Hopf bifurcation. Similarly, the classical Lotka-Volterra predator-prey model was studied in [8]. The results showed that the existence of time delay will change the stability of the equilibrium point, while the fear effect will stabilize the equilibrium point. Using the the center manifold reduction and normal form theory, formula for determining the stability and direction of Hopf bifurcation periodic solution was derived.

The paper is organized as follows. In Section 2, the time-space discrete Brusselator model is developed, and the existence and stability conditions of the equilibrium points are obtained. In Section 3, we give the parametric conditions for the Neimark-Sacker, flip and Turing bifurcation to occur. In Section 4, numerical simulations are presented to illustrate the theoretical results. The Turing instability region is also identified. In Section 5, we draw some conclusions.

2. Model and stability analysis

Prigogine and Lefever [23] proposed the following continuous-time Brusselator model

$$\begin{aligned} \dot{u}(t) &= a - (b+1)u(t) + u^2(t)v(t), \\ \dot{v}(t) &= bu(t) - u^2(t)v(t), \end{aligned} \tag{2.1}$$

where $u(t)$ and $v(t)$ are concentrations of activator and inhibitor respectively at time t; $a > 0$ and $b > 0$ represent the control parameters. Furthermore, note that in autocatalytic chemical reactions, the reactants often move from a region of high concentration to that of low concentration. From a mathematical point of view, this phenomenon can be described by diffusion. Given such considerations, it is necessary to introduce diffusion into the model. Therefore, the model with diffusion can be described as

$$\begin{aligned} \frac{\partial u(x,t)}{\partial t} &= a - (b+1)u(x,t) + u^2(x,t)v(x,t) + d_1\Delta u(x,t), \\ \frac{\partial v(x,t)}{\partial t} &= bu(x,t) - u^2(x,t)v(x,t) + d_2\Delta v(x,t), \end{aligned} \tag{2.2}$$

where Δ is the Laplacian operator, and the positive constants d_1 and d_2 are diffusion rates of activator and inhibitor respectively. In recent years, the effect of diffusion on dynamic behavior has been studied extensively. For example, in [19], Ma and Hu discussed the dynamic behavior of the continuous Brusselator system (2.2). They studied the global bifurcation of non-constant steady state solutions of the model by taking the concentration of a reactant as the bifurcation parameter, and described the local bifurcation with a specific example.

It is worth noting that the discrete time-space model described by the difference equation is more suitable than the continuous one due to its efficient calculation results and abundant dynamic behaviors. We note that the spatial pattern simulation algorithm is based on the discrete form corresponding to the continuous system. Therefore, it is frequent to use discrete model or effective discrete method to connect the real model and simulation. On the other hand, the dynamics of the Brusselator system in discrete time and space has not been studied much. Now, we will consider the simultaneous discretization of time and space to study the stability and bifurcation analysis of the Brusselator model.

Next, the CML model for system (2.2) will be presented. Define the time interval τ and the space interval δ. A two-dimensional matrix region is taken, which is divided into $n \times n$ grids by space intervals, where the (i,j) grid is only adjacent to the $(i+1,j),(i-1,j),(i,j+1)$ and $(i,j-1)$ grids. Continuous time t is divided by τ into a series of time intervals. Then, state variables $u_{(i,j,t)}$ and $v_{(i,j,t)}$ are defined, which represent the concentration of the activator and inhibitor in (i,j) position at the tth iteration. Assume the initial time is t_0, then tth iteration time is $t_0 + t_\tau$.

From [14,20,24,26], we know that in each discrete step from time t to $t+1$, the dynamic behaviors of the CML model consist of two parts, namely, the diffusion stage and the reaction stage. For the diffusion stage, we directly discretize the space term of system (2.2), and get

$$u'_{(i,j,t)} = u_{(i,j,t)} + \frac{\tau}{\delta^2} d_1 \Delta_d u_{(i,j,t)},$$

$$v'_{(i,j,t)} = v_{(i,j,t)} + \frac{\tau}{\delta^2} d_2 \Delta_d v_{(i,j,t)}, \tag{2.3}$$

where $u'_{(i,j,t)}$ and $v'_{(i,j,t)}$ mean the concentrations of activator and inhibitor after diffusion respectively, and Δ_d is the discretized Laplace operator of the following form

$$\begin{aligned} \Delta_d u_{(i,j,t)} &= u_{(i+1,j,t)} + u_{(i-1,j,t)} + u_{(i,j-1,t)} - 4u_{(i,j,t)}, \\ \Delta_d v_{(i,j,t)} &= v_{(i+1,j,t)} + v_{(i-1,j,t)} + v_{(i,j-1,t)} - 4v_{(i,j,t)}. \end{aligned} \tag{2.4}$$

Then, we discretize the reaction terms of equation (2.2) to obtain the reaction stage of the state variables $u_{(i,j,t)}$ and $v_{(i,j,t)}$

$$\begin{aligned} u_{(i,j,t+1)} &= f_1(u'_{(i,j,t)}, v'_{(i,j,t)}), \\ v_{(i,j,t+1)} &= g_1(u'_{(i,j,t)}, v'_{(i,j,t)}), \end{aligned} \tag{2.5}$$

in which

$$\begin{aligned} f_1(u,v) &= u + \tau[a - (b+1)u + u^2 v], \\ g_1(u,v) &= v + \tau(bu - u^2 v). \end{aligned}$$

Consider the following periodic boundary conditions

$$\begin{aligned} &u_{(i,0,t+1)} = u_{(i,n,t)}, u_{(i,1,t)} = u_{(i,n+1,t)}, u_{(0,j,t)} = u_{(n,j,t)}, u_{(i,j,t)} = u_{(n+1,j,t)}, \\ &v_{(i,0,t+1)} = v_{(i,n,t)}, v_{(i,1,t)} = v_{(i,n+1,t)}, v_{(0,j,t)} = v_{(n,j,t)}, v_{(i,j,t)} = v_{(n+1,j,t)}. \end{aligned} \tag{2.6}$$

The Brusselator system with discrete time and space has spatially homogeneous and heterogeneous dynamic properties. The homogeneous dynamics have the following property for all i, j and t

$$\Delta_d u_{(i,j,t)} = 0, \quad \Delta_d v_{(i,j,t)} = 0. \tag{2.7}$$

However, for the heterogeneous dynamics, there is at least a set of i, j, t, making $\Delta_d u_{(i,j,t)}$ and $\Delta_d v_{(i,j,t)}$ nonzero.

From the above analysis, the homogeneous dynamics are governed by the following equations

$$\begin{aligned} u_{t+1} &= u_t + \tau[a - (b+1)u_t + u_t^2 v_t], \\ v_{t+1} &= v_t + \tau(bu_t - u_t^2 v_t). \end{aligned} \tag{2.8}$$

We express equation (2.8) into a mapping

$$\begin{pmatrix} u \\ v \end{pmatrix} \mapsto \begin{pmatrix} u + \tau[a - (b+1)u + u^2 v] \\ v + \tau(bu - u^2 v) \end{pmatrix} \tag{2.9}$$

Now, we will use mapping (2.9) to analyze the homogeneous dynamics of equations (2.3)-(2.5). The equilibrium point of mapping (2.9) meets the following formulas

$$\begin{aligned} u &= u + \tau[a - (b+1)u + u^2 v], \\ v &= v + \tau(bu - u^2 v). \end{aligned} \tag{2.10}$$

By direct calculation, the unique positive equilibrium point is $(a, \frac{b}{a})$, which is denoted by (u^*, v^*). For the positive equilibrium point (u^*, v^*), the following proposition holds.

Proposition 2.1. *(1) If (S1) holds, it is a stable focus, where*

$$(S1)\begin{cases}(a-1)^2<b<(a+1)^2,\\ 0<\tau<\tau_N.\end{cases}$$

(2) If one of (S2) and (S3) holds, it is a stable degenerate node, where

$$(S2)\begin{cases}b=(a-1)^2,\\ 0<\tau<\tau_N.\end{cases}\qquad (S3)\begin{cases}b=(a+1)^2,\\ 0<\tau<\tau_N.\end{cases}$$

(3) If one of (S4) and (S5) holds, it is a stable node, where

$$(S4)\begin{cases}0<b<(a-1)^2,\\ 0<\tau<\tau_F.\end{cases}\qquad (S5)\begin{cases}b>(a+1)^2,\\ 0<\tau<\tau_F,\end{cases}$$

and $\tau_N=1-\frac{b-1}{a^2}$, $\tau_F=\tau_N-\sqrt{\tau_N^2-\frac{4}{a^2}}$.

Proof. The Jacobian matrix corresponding to any point (u,v) is

$$J(\tau)=\begin{bmatrix}1+\tau(2uv-b-1) & \tau u^2\\ \tau(b-2uv) & 1-\tau u^2\end{bmatrix}.$$

Then, it is easy to obtain that the eigenvalues evaluated at (u^*,v^*) are

$$\lambda_{1,2}(\tau)=\frac{1}{2}[-p(\tau)\pm\sqrt{p^2(\tau)-4q(\tau)}] \tag{2.11}$$

with

$$\begin{aligned}p(\tau)=&-2+(a^2-b+1)\tau,\\ q(\tau)=&1-(a^2-b+1)\tau+a^2\tau^2.\end{aligned} \tag{2.12}$$

Therefore, if $|\lambda_1|<1$ and $|\lambda_2|<1$ hold, then (u^*,v^*) is asymptotically stable. That is,

$$q(\tau)<1,\quad |p(\tau)|<1+q(\tau). \tag{2.13}$$

By solving (2.13) and from [21], the above results can be obtained. □

3. Bifurcation analysis

Now, bifurcation phenomena will be discussed at the equilibrium point (u^*,v^*). τ will be taken as the main bifurcation parameter, and occurrence conditions for three bifurcation at (u^*,v^*) will be established, namely, Neimark-Sacker, flip and Turing bifurcation.

3.1. Neimark-Sacker bifurcation

From the literature such as [22,27,32], if the Neimark-Sacker bifurcation is experienced at the equilibrium point (u^*, v^*), then the eigenvalues of the Jacobian matrix $J(\tau)$ must have a pair of conjugate complex roots $\lambda_{1,2}$, with module 1. It means that $p^2(\tau) - 4q(\tau) < 0$ and $q(\tau) = 1$. That is,

$$\begin{cases} (a-1)^2 < b < (a+1)^2, \\ \tau = \tau_N, \end{cases} \tag{3.1}$$

where τ_N is the threshold value.

One rewrites (2.11) as follows

$$\lambda_{1,2}(\tau) = \frac{-p(\tau)}{2} \pm \frac{i}{2}\sqrt{4q(\tau) - p^2(\tau)} \triangleq \alpha_1 \pm \alpha_2 i. \tag{3.2}$$

Now, we need to verify that the transversality condition for the occurrence of Neimark-Sacker bifurcation is true. In fact,

$$d = \frac{d|\lambda(\tau)|}{d\tau}\Big|_{\tau=\tau_N} = a^2 - b + 1 > 0. \tag{3.3}$$

Besides, the condition $\lambda(\tau_N)^n \neq 1, n = 1, 2, 3, 4$ needs to be satisfied for the Neimark-Sacker bifurcation, which implies $p(\tau_N) \neq -2, 0, 1, 2$. Since $p^2(\tau_N) - 4 < 0$, one yields $p(\tau_N) \neq -2, 2$. Hence, $p(\tau_N) \neq 0, 1$ holds, i.e.,

$$(a^2 - b + 1)\tau_N \neq 2, 3. \tag{3.4}$$

Under the above conditions, we translate the equilibrium point (u^*, v^*) of mapping (2.9) into the origin. Let $w = u - u^*, z = v - v^*$ and $\tau = \tau_N$, then we rewrite mapping (2.9), and get

$$\begin{aligned} \begin{pmatrix} w \\ z \end{pmatrix} \mapsto & \begin{pmatrix} a_{10} & a_{01} \\ b_{10} & b_{01} \end{pmatrix} \begin{pmatrix} w \\ z \end{pmatrix} \\ & + \begin{pmatrix} a_{20}w^2 + a_{11}wz + a_{21}w^2z + a_{30}w^3 + O((|w| + |z|)^4) \\ b_{20}w^2 + b_{11}wz + b_{21}w^2z + b_{30}w^3 + O((|w| + |z|)^4) \end{pmatrix}, \end{aligned} \tag{3.5}$$

where

$$\begin{aligned} & a_{10} = 1 + (b-1)\tau_N, \quad a_{01} = a^2\tau_N, \quad a_{20} = \frac{b}{a}\tau_N, \quad a_{11} = 2a\tau_N, \\ & a_{21} = \tau_N, \quad a_{30} = 0, \quad b_{10} = -b\tau_N, \quad b_{01} = 1 - a^2\tau_N, \\ & b_{20} = -\frac{b}{a}\tau_N, \quad b_{11} = -2a\tau_N, \quad b_{21} = -\tau_N, \quad b_{30} = 0. \end{aligned} \tag{3.6}$$

The normal form of mapping (3.5) will be given below. To this end, nonsingular coordinate transformation is introduced. We let

$$\begin{pmatrix} w \\ z \end{pmatrix} = \begin{pmatrix} a_{01} & 0 \\ \alpha_1 - a_{10} & -\alpha_2 \end{pmatrix} \begin{pmatrix} \bar{w} \\ \bar{z} \end{pmatrix}. \tag{3.7}$$

From mapping (3.5), the following results can be obtained

$$\begin{pmatrix} \bar{w} \\ \bar{z} \end{pmatrix} \mapsto \begin{pmatrix} \alpha_1 & -\alpha_2 \\ \alpha_2 & \alpha_1 \end{pmatrix} \begin{pmatrix} \bar{w} \\ \bar{z} \end{pmatrix} + \frac{1}{a_{01}\alpha_2} \begin{pmatrix} G_1(\bar{w}, \bar{z}) \\ G_2(\bar{w}, \bar{z}) \end{pmatrix}. \tag{3.8}$$

Then, one can get

$$\begin{pmatrix} G_1(\bar{w}, \bar{z}) \\ G_2(\bar{w}, \bar{z}) \end{pmatrix} = \begin{pmatrix} \alpha_2 & 0 \\ \alpha_1 - a_{10} & -a_{01} \end{pmatrix} \times \begin{pmatrix} a_{20}w^2 + a_{11}wz + a_{21}w^2z + a_{30}w^3 + O((|w| + |z|)^4) \\ b_{20}w^2 + b_{11}wz + b_{21}w^2z + b_{30}w^3 + O((|w| + |z|)^4) \end{pmatrix}.$$

Rearranging the above equation, one yields the expressions of $G_1(\bar{w}, \bar{z})$ and $G_2(\bar{w}, \bar{z})$ as follows

$$\begin{aligned} G_1(\bar{w}, \bar{z}) =& [a_{20}a_{01}^2 + a_{11}a_{01}(\alpha_1 - a_{10})]\alpha_2\bar{w}^2 - \alpha_2^2 a_{11}a_{01}\bar{w}\bar{z} \\ &+ [(\alpha_1 - a_{10})a_{21} + a_{30}a_{01}]a_{01}^2\alpha_2\bar{w}^3 - \alpha_2^2 a_{21}a_{01}^2\bar{w}^2\bar{z} + O((|w| + |z|)^4), \\ G_2(\bar{w}, \bar{z}) =& [(\alpha_1 - a_{10})(a_{11}((\alpha_1 - a_{10}) + a_{01}(a_{20} - b_{11}))a_{01} - b_{20}a_{01}^2]a_{01}\bar{w}^2 \\ &+ [(\alpha_1 - a_{10})(a_{21}(\alpha_1 - a_{10}) + a_{01}(a_{30} - b_{21})) - b_{30}a_{01}^2]a_{01}^2\bar{w}^3 \\ &- (a_{11}(\alpha_1 - a_{10}) - a_{10}b_{11})\alpha_2 a_{01}\bar{w}\bar{z} \\ &- (a_{21}(\alpha_1 - a_{10}) - b_{21}a_{01})\alpha_2 a_{01}^2\bar{w}^2\bar{z} + O((|w| + |z|)^4). \end{aligned}$$

Thereby, the second and third partial derivatives of $G_1(\bar{w}, \bar{z})$ and $G_2(\bar{w}, \bar{z})$ with respect to $(\bar{w}, \bar{z})$ could be evaluated at $(0, 0)$.

$$\begin{aligned} &G_{1\bar{w}\bar{w}} = 2[a_{20}a_{01}^2 + a_{11}a_{01}(\alpha_1 - a_{10})]\alpha_2, \\ &G_{1\bar{w}\bar{z}} = -\alpha_2^2 a_{11}a_{01}, \\ &G_{2\bar{w}\bar{w}} = 2[(\alpha_1 - a_{10})^2 a_{11} - a_{01}((\alpha_1 - a_{10})(b_{11} - a_{20}) + a_{01}b_{20})]a_{01}, \\ &G_{2\bar{w}\bar{z}} = [a_{01}^2 b_{11} - (\alpha_1 - a_{10})a_{01}a_{11}]\alpha_2, \\ &G_{1\bar{w}\bar{w}\bar{w}} = 6[(\alpha_1 - a_{10})a_{01}^2 a_{21} + a_{01}^3 a_{30}]\alpha_2, \\ &G_{1\bar{w}\bar{w}\bar{z}} = -2\alpha_2^2 a_{21}a_{01}^2, \\ &G_{2\bar{w}\bar{w}\bar{w}} = 6[(\alpha_1 - a_{10})^2 a_{21} - a_{01}((\alpha_1 - a_{10})(b_{21} - a_{30}) + a_{01}b_{30})]a_{01}^2, \\ &G_{2\bar{w}\bar{w}\bar{z}} = 2[a_{01}b_{21} - (\alpha_1 - a_{10})a_{21}]a_{01}^2\alpha_2, \\ &G_{1\bar{z}\bar{z}} = 0, \quad G_{1\bar{w}\bar{z}\bar{z}} = 0, \quad G_{1\bar{z}\bar{z}\bar{z}} = 0, \quad G_{2\bar{z}\bar{z}} = 0, \quad G_{2\bar{w}\bar{z}\bar{z}} = 0, \quad G_{2\bar{z}\bar{z}\bar{z}} = 0. \end{aligned}$$

Now, it is necessary to verify that the discriminatory quantity ξ is not equal to 0 from [10, 32]. That is,

$$\xi = -Re\{\frac{(1 - 2\lambda)\bar{\lambda}^2}{1 + \lambda}\zeta_{11}\zeta_{20}\} - \frac{1}{2}|\zeta_{11}|^2 - |\zeta_{02}|^2 + Re\{\bar{\lambda}\zeta_{21}\} \neq 0 \tag{3.9}$$

with

$$\zeta_{20} = \frac{1}{8a_{01}\alpha_2}[G_{1\bar{w}\bar{w}} - G_{1\bar{z}\bar{z}} + 2G_{2\bar{w}\bar{z}} + i(G_{2\bar{w}\bar{w}} - G_{2\bar{z}\bar{z}} - 2G_{1\bar{w}\bar{z}})],$$

$$\zeta_{11} = \frac{1}{4a_{01}\alpha_2}[G_{1\bar{w}\bar{z}} + G_{1\bar{z}\bar{z}} + i(G_{2\bar{w}\bar{w}} + G_{2\bar{z}\bar{z}})],$$
$$\zeta_{02} = \frac{1}{8a_{01}\alpha_2}[G_{1\bar{w}\bar{w}} - G_{1\bar{z}\bar{z}} - 2G_{2\bar{w}\bar{z}} + i(G_{2\bar{w}\bar{w}} - G_{2\bar{z}\bar{z}} + 2G_{1\bar{w}\bar{z}})],$$
$$\zeta_{21} = \frac{1}{16a_{01}\alpha_2}[G_{1\bar{w}\bar{w}\bar{w}} + G_{1\bar{w}\bar{z}\bar{z}} + G_{2\bar{w}\bar{w}\bar{z}} + G_{2\bar{z}\bar{z}\bar{z}} + i(G_{2\bar{z}\bar{z}\bar{z}} + G_{2\bar{w}\bar{z}\bar{z}} - G_{1\bar{w}\bar{w}\bar{z}} - G_{1\bar{z}\bar{z}\bar{z}})].$$

Therefore, we have

$$\begin{aligned}\xi = &-\frac{B}{A}G_{1\bar{w}\bar{w}}(G_{1\bar{w}\bar{w}} + 2(G_{2\bar{w}\bar{w}}) - \frac{C}{A}G_{1\bar{w}\bar{w}}(G_{2\bar{w}\bar{w}} - 2G_{1\bar{w}\bar{z}})\\ &- \frac{C}{A}G_{2\bar{w}\bar{w}}(G_{1\bar{w}\bar{w}} + 2G_{2\bar{w}\bar{w}}) + \frac{B}{A}G_{2\bar{w}\bar{w}}(G_{2\bar{w}\bar{w}} - 2G_{1\bar{w}\bar{Z}})\\ &- \frac{1}{32a_{01}^2\alpha_2^2}(G_{1\bar{w}\bar{w}}^2 + G_{2\bar{w}\bar{w}}^2) - \frac{1}{64a_{01}^2\alpha_2^2}[(G_{1\bar{w}\bar{w}} - 2G_{2\bar{w}\bar{z}})^2\\ &+ (G_{2\bar{w}\bar{w}} + 2G_{1\bar{w}\bar{z}})^2] + \frac{1}{16a_{01}\alpha_2}[\alpha_1(G_{1\bar{w}\bar{w}\bar{w}} + G_{2\bar{w}\bar{w}\bar{z}}) + \alpha_2(G_{2\bar{w}\bar{w}\bar{w}} - G_{1\bar{w}\bar{w}\bar{z}})]\end{aligned}$$

and

$$\begin{aligned}A =&32a_{01}^2\alpha_2^2[(1-\alpha_1)^2 + \alpha_2^2],\\ B =&\alpha_1^2 - 3\alpha_1^3 + 2\alpha_1^4 - \alpha_2^2 + \alpha_1\alpha_2^2 - 2\alpha_2^4,\\ C =&2\alpha_1\alpha_2 - 5\alpha_1^2\alpha_2 + 4\alpha_1^3\alpha_2 - \alpha_2^3 + 4\alpha_1\alpha_2^3.\end{aligned}$$

From the above analysis results, the following statements are valid.

Theorem 3.1. *Suppose conditions (S11) $(a-1)^2 < b < (a+1)^2$ and (3.4) are satisfied. When $\xi \neq 0$, then mapping (2.9) undergoes Neimark-Sacker bifurcation at the equilibrium point (u^*, v^*) as $\tau = \tau_N$. Furthermore, when $\xi < 0$, then an attracting invariant circle bifurcates from (u^*, v^*) for $\tau > \tau_N$; when $\xi > 0$, then a repelling invariant circle bifurcates from (u^*, v^*) for $0 < \tau < \tau_N$.*

3.2. Flip bifurcation

From [10], we know that if mapping (2.9) admits the flip bifurcation, it requires $q(\tau) = p(\tau) - 1$, where $p(\tau)$ and $q(\tau)$ are given in (2.12). Therefore, the threshold value τ_F of the flip bifurcation can be obtained

$$\tau_F = \tau_N - \sqrt{\tau_N^2 - \frac{4}{a^2}}.$$

It is not difficult to see that at $\tau = \tau_F$, and two eigenvalues are $\lambda_1 = -1$, $\lambda_2 = 1 - p(\tau_F)$. The flip bifurcation also requires $|\lambda_2| \neq 1$. By calculation, we can get

$$(a^2 - b + 1)\tau_F \neq 2, 4. \tag{3.10}$$

Now, let us shift the equilibrium point of mapping (2.9) to the origin. Let $w = u - u^*$, $z = v - v^*$, and $\tilde{\tau} = \tau - \tau_F$, then mapping (2.9) becomes

$$\begin{pmatrix} w \\ \tilde{\tau} \\ z \end{pmatrix} \mapsto \begin{pmatrix} a_{100} & 0 & a_{001} \\ 0 & 1 & 0 \\ b_{100} & 0 & b_{001} \end{pmatrix} \begin{pmatrix} w \\ \tilde{\tau} \\ z \end{pmatrix} + \begin{pmatrix} f_1(w, \tilde{\tau}, z) \\ 0 \\ g_1(w, \tilde{\tau}, z) \end{pmatrix}, \tag{3.11}$$

where

$$\begin{aligned} f_1(w,\tilde{\tau},z) =& a_{200}w^2 + a_{101}wz + a_{110}w\tilde{\tau} + a_{011}\tilde{\tau}z + a_{210}w^2\tilde{\tau} + a_{111}w\tilde{\tau}z \\ &+ a_{300}w^3 + a_{201}w^2z + O((|w| + |\tilde{\tau}| + |z|)^4), \\ g_1(w,\tilde{\tau},z) =& b_{200}w^2 + b_{101}wz + b_{110}w\tilde{\tau} + b_{011}\tilde{\tau}z + b_{210}w^2\tilde{\tau} + b_{111}w\tilde{\tau}z \\ &+ b_{300}w^3 + b_{201}w^2z + O((|w| + |\tilde{\tau}| + |z|)^4) \end{aligned}$$

and

$$\begin{aligned} &a_{100} = 1 + (b-1)\tau_F, \quad a_{001} = a^2\tau_F, \quad a_{200} = \frac{b}{a}\tau_F, \quad a_{101} = 2a\tau_F, \\ &a_{110} = b - 1, \quad a_{011} = a^2, \quad a_{210} = \frac{b}{a}, \quad a_{111} = 2a, \quad a_{300} = 0, \\ &a_{201} = \tau_F, \quad b_{100} = -b\tau_F, \quad b_{001} = 1 - a^2\tau_F, \quad b_{200} = -\frac{b}{a}\tau_F, \\ &b_{101} = -2a\tau_F, \quad b_{110} = -b, \quad b_{011} = -a^2, \quad b_{210} = -\frac{b}{a}, \\ &b_{111} = -2a, \quad b_{300} = 0, \quad b_{201} = -\tau_F. \end{aligned}$$

One introduces an invertible matrix

$$T = \begin{pmatrix} a_{001} & 0 & a_{001} \\ 0 & 1 & 0 \\ -1 - a_{100} & 0 & \lambda_2 - a_{100} \end{pmatrix}. \tag{3.12}$$

Let

$$\begin{pmatrix} w \\ \tilde{\tau} \\ z \end{pmatrix} = T \begin{pmatrix} \bar{w} \\ \tilde{\tau} \\ \bar{z} \end{pmatrix}. \tag{3.13}$$

From equations (3.11)-(3.13) and $\lambda_2 = 1 - p(\tau_F)$, one has

$$\begin{pmatrix} \bar{w} \\ \tilde{\tau} \\ \bar{z} \end{pmatrix} \mapsto \begin{pmatrix} -1 & & \\ & 1 & \\ & & \lambda_2 \end{pmatrix} \begin{pmatrix} \bar{w} \\ \tilde{\tau} \\ \bar{z} \end{pmatrix} + \begin{pmatrix} \tilde{F}_1(\bar{w},\tilde{\tau},\bar{z}) \\ 0 \\ \tilde{G}_1(\bar{w},\tilde{\tau},\bar{z}) \end{pmatrix} \tag{3.14}$$

and

$$\begin{pmatrix} \tilde{F}_1(\bar{w},\tilde{\tau},\bar{z}) \\ 0 \\ \tilde{G}_1(\bar{w},\tilde{\tau},\bar{z}) \end{pmatrix} = T^{-1} \begin{pmatrix} f_1(T(\bar{w},\tilde{\tau},\bar{z})) \\ 0 \\ g_1((T(\bar{w},\tilde{\tau},\bar{z})) \end{pmatrix}.$$

It is found that

$$\tilde{F}_1(\bar{w},\tilde{\tau},\bar{z}) = \frac{1}{(1+\lambda_2)}[[a_{001}a_{200}(\lambda_2 - a_{100}) - a_{001}^2 b_{200}](\bar{w} + \bar{z})^2]$$

$$
\begin{aligned}
&+\frac{1}{(1+\lambda_2)}[[(\lambda_2-a_{100})a_{110}-a_{001}b_{100}](\bar{w}+\bar{z})\tilde{\tau}]\\
&+\frac{a_{001}^2}{(1+\lambda_2)}[(\lambda_2-a_{100})a_{300}-a_{001}b_{300}](\bar{w}+\bar{z})^3\\
&+\frac{a_{001}}{(1+\lambda_2)}[(\lambda_2-a_{100})a_{210}-a_{001}b_{210}](\bar{w}+\bar{z})^2\tilde{\tau}\\
&+\frac{a_{011}(\lambda_2-a_{100})}{a_{001}(1+\lambda_2)}[(-1-a_{100})\bar{w}+(\lambda_2-a_{100})\bar{z}]\tilde{\tau}\\
&+\frac{1}{(1+\lambda_2)}[(\lambda_2-a_{100})a_{101}-a_{001}b_{101}]\\
&\times[(-1-a_{100})\bar{w}+(\lambda_2-a_{100})\bar{z}](\bar{w}+\bar{z})\\
&+\frac{1}{(1+\lambda_2)}[a_{111}(\lambda_2-a_{100})-a_{001}b_{111}]\\
&\times[(-1-a_{100})\bar{w}+(\lambda_2-a_{100})\bar{z}](\bar{w}+\bar{z})\tilde{\tau}\\
&+\frac{a_{001}}{(1+\lambda_2)}[(\lambda_2-a_{100})a_{201}-a_{001}b_{201}]\\
&\times[(-1-a_{100})\bar{w}+(\lambda_2-a_{100})\bar{z}](\bar{w}+\bar{z})^2+O((|w|+|\tilde{\tau}|+|z|)^4),
\end{aligned}
$$

$$
\begin{aligned}
\tilde{G}_1(\bar{w},\tilde{\tau},\bar{z}) = {}& \frac{1}{(1+\lambda_2)}a_{001}a_{200}(1+a_{100})+a_{001}^2b_{200}](\bar{w}+\bar{z})^2\\
&+\frac{1}{(1+\lambda_2)}[a_{110}(1+a_{100})+a_{001}b_{110}](\bar{w}+\bar{z})\tilde{\tau}\\
&+\frac{a_{001}^2}{(1+\lambda_2)}[(1+a_{100})a_{300}+a_{001}b_{300}](\bar{w}+\bar{z})^3\\
&+\frac{a_{001}}{(1+\lambda_2)}[(1+a_{100})a_{210}+a_{001}b_{210}](\bar{w}+\bar{z})^2\tilde{\tau}\\
&+\frac{a_{011}(1+a_{100})}{a_{001}(1+\lambda_2)}[(-1-a_{100})\bar{w}+(\lambda_2-a_{100})\bar{z}]\tilde{\tau}\\
&+\frac{1}{(1+\lambda_2)}[(1+a_{100})a_{101}+a_{001}b_{101}][(-1-a_{100})\bar{w}+(\lambda_2-a_{100})\bar{z}](\bar{w}+\bar{z})\\
&+\frac{1}{(1+\lambda_2)}[a_{111}(1+a_{100})+a_{001}b_{111}][(-1-a_{100})\bar{w}+(\lambda_2-a_{100})\bar{z}](\bar{w}+\bar{z})\tilde{\tau}\\
&+\frac{a_{001}}{(1+\lambda_2)}[(1+a_{100})a_{201}+a_{001}b_{201}]\\
&\times[(-1-a_{100})\bar{w}+(\lambda_2-a_{100})\bar{z}](\bar{w}+\bar{z})^2+O((|w|+|\tilde{\tau}|+|z|)^4).
\end{aligned}
$$

Present the center manifold $\mathcal{W}^c(0,0,0)$ at the fixed point $(0,0,0)$ as follows

$$\mathcal{W}^c(0,0,0)=\{(\bar{w},\tilde{\tau},\bar{z})\in R^3|\bar{z}=s(\bar{w},\tilde{\tau}),s(0,0)=0,Ds(0,0)=0\}$$

with $s(\bar{w},\tilde{\tau})=k_0\bar{w}^2+k_1\bar{w}\tilde{\tau}+k_2\tilde{\tau}^2+O((|\bar{w}|+|\tilde{\tau}|)^3)$.

Substituting $\bar{z}=s(\bar{w},\tilde{\tau})$ into mapping (3.14) and from the invariance of the local center manifold, one obtains

$$
\begin{aligned}
&\lambda_2(k_0\bar{w}^2+k_1\bar{w}\tilde{\tau}+k_2\tilde{\tau}^2)+\tilde{G}_1(\bar{w},\tilde{\tau},\bar{z})\\
&=k_0(-\tilde{w}+\tilde{F}_1(\bar{w},\tilde{\tau},s(\bar{w},\tilde{\tau})))^2+k_1(-\tilde{w}+\tilde{F}_1(\bar{w},\tilde{\tau},s(\bar{w},\tilde{\tau})))\tilde{\tau}
\end{aligned}
$$

$$+ k_2\tilde{\tau}^2 + O((|\bar{w}| + |\tilde{\tau}|)^3). \tag{3.15}$$

Comparing the coefficients of $\bar{w}^2$, $\bar{w}\tilde{\tau}$ and $\tilde{\tau}^2$ on both sides of the above equation, we yield

$$\begin{aligned}
k_0 &= \frac{1}{\lambda_2^2 - 1}[(1 + a_{100})^2 a_{101} - a_{001}(1 + a_{100})(a_{200} - b_{101}) - a_{001}^2 b_{200}],\\
k_1 &= \frac{1}{a_{001}(\lambda_2 + 1)^2}[(1 + a_{100})^2 a_{011} - a_{001}a_{110}(1 + a_{100}) - a_{001}^2 b_{110}],\\
k_2 &= 0.
\end{aligned}$$

When mapping (3.14) is restricted into the center manifold $\mathcal{W}^c(0, 0, 0)$, it is not difficult to obtain the following mapping

$$\begin{aligned}
\mathcal{F} : \bar{w} \mapsto & -\bar{w} + x_{20}\bar{w}^2 + x_{11}\bar{w}\tilde{\tau} + x_{21}\bar{w}^2\tilde{\tau} + x_{12}\bar{w}\tilde{\tau}^2 + x_{30}\bar{w}^3\\
& + O((|\bar{w}| + |\tilde{\tau}|)^4),
\end{aligned} \tag{3.16}$$

where

$$\begin{aligned}
x_{20} &= (1 - \frac{2}{1 + \lambda_2})(a_{001}b_{101} - 2a_{101}) - \frac{1}{1 + \lambda_2}(a_{001}^2 b_{200} - 2a_{001}a_{200}),\\
x_{11} &= \frac{1}{1 + \lambda_2}[(2a_{110} - \frac{2a_{011(1+a_{100})}}{a_{001}} - a_{001}b_{110}],\\
x_{21} &= \frac{1}{(1 + \lambda_2)a_{001}}(4a_{011} + 2a_{001}a_{110} - a_{001}^2 b_{110})k_0\\
&\quad + \frac{1}{(1 + \lambda_2)a_{001}}[2a_{001}(2a_{101} + 2a_{001}a_{200} - a_{001}^2 b_{200} - a_{001}b_{101})\\
&\quad + (1 + a_{100}a_{001}(a_{001}b_{101} - 2a_{101})]k_1 + \frac{1}{(1 + \lambda_2)a_{001}}[a_{001}^2(2a_{210} - a_{001}b_{210})\\
&\quad + (1 + a_{100}) \times (a_{001}^2 b_{111} - 2a_{001}a_{111})],\\
x_{12} &= \frac{1}{(1 + \lambda_2)}(\frac{4a_{011}}{a_{001}} + 2a_{110} - a_{001}b_{110})k_1,\\
x_{30} &= \frac{1}{(1 + \lambda_2)}[(4a_{101} + 4a_{001}a_{200} - a_{001}^2 b_{200} - 2a_{001}b_{101})\\
&\quad + (a_{001}b_{101} - 2a_{101})(1 + a_{100})]k_0\\
&\quad + \frac{a_{001}}{(1 + \lambda_2)}[(2a_{001}a_{300} - a_{001}^2 b_{300}) + (1 + a_{100})(a_{001}b_{201} - 2a_{201})].
\end{aligned}$$

Now, let us verify the last condition of the flip bifurcation in [10] $\eta_1 \neq 0$ and $\eta_2 \neq 0$, i.e.,

$$\begin{aligned}
\eta_1 &= (\frac{\partial^2 \mathcal{F}}{\partial \bar{w}\partial\tilde{\tau}} + \frac{1}{2}\frac{\partial \mathcal{F}}{\partial \tilde{\tau}}\frac{\partial^2 \mathcal{F}}{\partial \bar{w}^2})\Big|_{(\bar{w},\tilde{\tau})=(0,0)} \neq 0,\\
\eta_2 &= (\frac{1}{6}\frac{\partial^3 \mathcal{F}}{\partial \bar{w}^3} + (\frac{1}{2}\frac{\partial^2 \mathcal{F}}{\partial \bar{w}^2})^2)\Big|_{(\bar{w},\tilde{\tau})=(0,0)} \neq 0.
\end{aligned}$$

The calculation gives us $\eta_1 = x_{11} \neq 0$, $\eta_2 = x_{30} + x_{20}^2 \neq 0$. Therefore, the following theorem can be yielded.

Theorem 3.2. *Under the condition that equation (3.10) is true, supposing one of the conditions*

$$(S41): 0 < b < (a-1)^2, \qquad (S51): b > (a+1)^2$$

is satisfied, then we have

(1) when $\eta_1 \neq 0$, $\eta_2 \neq 0$ and $\tau = \tau_F$, then mapping (2.9) experiences the flip bifurcation at the equilibrium point (u^*, v^*);

(2) when $\eta_2 < 0$, then an unstable periodic-2 orbit bifurcates from (u^*, v^*);

(3) when $\eta_2 > 0$, then a stable periodic-2 orbit bifurcates from (u^*, v^*).

3.3. Turing bifurcation

Two necessary conditions are needed for the Turing bifurcation to occur (see [1, 5, 14]). First, there is a nontrivial homogeneous state which is stable in time. It is noted that if one of conditions $(S1) - (S5)$ is guaranteed, (u^*, v^*) is stable. Then, we need to confirm that the stable nontrivial homogeneous steady state becomes unstable under spatial heterogeneous perturbations. Here, we will discuss the Turing bifurcation of homogeneous stationary states by assuming one of conditions $(S1) - (S5)$ holds. In order to obtain conditions that support Turing instability, the eigenfunction of the Laplace operator Δ_d is defined

$$\Delta_d X^{ij} + \lambda_{kl} X^{ij} = 0, \quad i, j = 1, 2, 3, \cdots, \tag{3.17}$$

and the periodic boundary condition is

$$X^{i,0} = X^{i,n}, X^{i,1} = X^{i,n+1}, X^{0,j} = X^{n,j}, X^{1,j} = X^{n+1,j}.$$

From [2], the eigenvalue λ_{kl} of Δ_d satisfies the following condition

$$\lambda_{kl} = 4(sin^2 \frac{(k-1)\pi}{n} + sin^2 \frac{(l-1)\pi}{n}), \quad k, l = 1, 2, 3, \cdots.$$

Now, the small spatial heterogeneous disturbances $\tilde{u}_{(i,j,t)}$ and $\tilde{v}_{(i,j,t)}$ are added to the homogeneous steady state. Let $\tilde{u}_{(i,j,t)} = u_{(i,j,t)} - u^*$, $\tilde{v}_{(i,j,t)} = v_{(i,j,t)} - u^*$, it is natural to get $\Delta_d \tilde{u}_{(i,j,t)} = \Delta_d u_{(i,j,t)}$ and $\Delta_d \tilde{v}_{(i,j,t)} = \Delta_d v_{(i,j,t)}$. Plugging the above equations into (2.3)-(2.5), then one yields

$$\begin{aligned}
\tilde{u}_{(i,j,t+1)} &= a_{10}(\tilde{u}_{(i,j,t)} + \frac{\tau}{\delta^2} d_1 \Delta_d \tilde{u}_{(i,j,t)}) + a_{01}(\tilde{v}_{(i,j,t)} + \frac{\tau}{\delta^2} d_2 \Delta_d \tilde{v}_{(i,j,t)}) \\
&\quad + O((|\tilde{u}_{(i,j,t)}| + |\tilde{v}_{(i,j,t)}|)^2), \\
\tilde{v}_{(i,j,t+1)} &= b_{10}(\tilde{u}_{(i,j,t)} + \frac{\tau}{\delta^2} d_1 \Delta_d \tilde{u}_{(i,j,t)}) + b_{01}(\tilde{v}_{(i,j,t)} + \frac{\tau}{\delta^2} d_2 \Delta_d \tilde{v}_{(i,j,t)}) \\
&\quad + O((|\tilde{u}_{(i,j,t)}| + |\tilde{v}_{(i,j,t)}|)^2).
\end{aligned} \tag{3.18}$$

Assume that X^{ij}_{kl} is an eigenfunction of the eigenvalue λ_{kl}. Equation (3.18) is multiplied by X^{ij}_{kl}. Summing over all i, j, we have

$$\begin{aligned}
\Sigma X^{ij}_{kl} \tilde{u}_{(i,j,t+1)} &= a_{10} \Sigma X^{ij}_{kl} \tilde{u}_{(i,j,t)} + a_{01} \Sigma X^{ij}_{kl} \tilde{v}_{(i,j,t)} \\
&\quad + \frac{\tau}{\delta^2} a_{10} d_1 \Sigma X^{ij}_{kl} \Delta_d \tilde{u}_{(i,j,t)} + \frac{\tau}{\delta^2} a_{01} d_2 \Delta_d \tilde{v}_{(i,j,t)},
\end{aligned}$$

$$\Sigma X_{kl}^{ij}\tilde{v}_{(i,j,t+1)} = b_{10}\Sigma X_{kl}^{ij}\tilde{u}_{(i,j,t)} + b_{01}\Sigma X_{kl}^{ij}\tilde{v}_{(i,j,t)} + \frac{\tau}{\delta^2}b_{10}d_1\Sigma X_{kl}^{ij}\Delta_d\tilde{u}_{(i,j,t)} + \frac{\tau}{\delta^2}b_{01}d_2\Delta_d\tilde{v}_{(i,j,t)}.$$

For the sake of convenience, we set

$$U_t = \Sigma X_{kl}^{ij}\tilde{u}_{(i,j,t)},$$
$$V_t = \Sigma X_{kl}^{ij}\tilde{v}_{(i,j,t)}.$$

Thereby, one yields

$$U_{t+1} = a_{10}(1 - \frac{\tau}{\delta^2}d_1\lambda_{kl})U_t + a_{01}(1 - \frac{\tau}{\delta^2}d_2\lambda_{kl})V_t,$$
$$V_{t+1} = b_{10}(1 - \frac{\tau}{\delta^2}d_1\lambda_{kl})U_t + b_{01}(1 - \frac{\tau}{\delta^2}d_2\lambda_{kl})V_t. \tag{3.19}$$

In fact, discrete system (3.19) describes the dynamic sum of the spatial inhomogeneous perturbations over all discrete lattices in the whole two-dimensional space. That implies when equation (3.19) diverges, the spatial symmetry of the discrete Brusselator system is broken at the equilibrium point (u^*, v^*), which will lead to the formation of the Turing pattern. From a simple calculation, the equilibrium point of equation (3.19) is $(0, 0)$ and the eigenvalues at $(0, 0)$ are

$$\lambda_{\pm}(k, l, \tau) = \frac{1}{2}R_1(k, l, \tau) \pm \frac{1}{2}\sqrt{R_1(k, l, \tau) - 4R_2(k, l, \tau)}, \tag{3.20}$$

where

$$R_1(k, l, \tau) = a_{10} + b_{01} - \frac{\tau}{\delta^2}\lambda_{kl}(a_{10}d_1 + b_{01}d_2),$$
$$R_2(k, l, \tau) = (a_{10}b_{01} - a_{01}b_{10})(1 - \frac{\tau}{\delta^2}d_1\lambda_{kl})(1 - \frac{\tau}{\delta^2}d_2\lambda_{kl}).$$

Besides, the occurrence of Turing instability requires that the maximum value of $|\lambda_{\pm}(k, l, \tau)|$ be greater than one. Denote

$$Z(k, l, \tau) = \max\{|\lambda_{\pm}(k, l, \tau)|\},$$
$$Z_m(\tau) = \max_{k=1,l=1}^{n} Z(k, l, \tau), ((k, l) \neq (1, 1)). \tag{3.21}$$

Therefore, we can figure out the critical value τ_T of the Turing bifurcation by solving $Z_m = 1$. From (3.21), we know that if τ is close to τ_T, when $R_1^2(k, l, \tau) > 4R_2(k, l, \tau)$, τ_T meets

$$\max_{k=1,l=1}^{n}\{|R_1(k, l, \tau_T|) - R_2(k, l, \tau_T)\} = 1;$$

when $R_1^2(k, l, \tau) \leq 4R_2(k, l, \tau)$, τ_T meets

$$R_2(k, l, \tau_T) = 1.$$

As a result, we have the following conclusions.

Theorem 3.3. *Assume that one of conditions $(S1) - (S5)$ is satisfied, and τ is in a small neighborhood of τ_T,*

(1) when $Z_m > 1$, the homogeneous steady state of the CML model (2.2)-(2.5) with periodic boundary conditions experiences Turing instability, and the Turing pattern is formed;

(2) when $Z_m < 1$, the homogeneous steady state of the CML model remains stable, and no Turing pattern will be formed.

4. Numerical simulation

In this section, we will verify the dynamic evolution of the Neimark-Sacker bifurcation, flip bifurcation and Turing instability through numerical simulations. Also, the associated spatiotemporal patterns are presented.

4.1. Neimark-Sacker bifurcation and related Turing patterns

Set $a = 0.963$ and $b = 0.94$. By direct calculation, we note that this set of parameters satisfies conditions (S11) and (3.4), and the equilibrium point is $(u^*, v^*) = (0.963, 0.9761)$ and $\tau_N = 1.0647$. It is important to note that the values of τ we take next are all near τ_N.

Let $\tau = 1.015 < \tau_N$, since $\lambda_{1,2} = 0.5376 \pm 0.6427i$, $|\lambda_{1,2}| \approx 0.4131 < 1$, the equilibrium point (u^*, v^*) is asymptotically stable. When $\tau = \tau_N = 1.0647$, we have discriminatory quantity $\xi = -1.5369$. Hence, when $\tau = \tau_N$, the discrete system experiences Neimark-Sacker bifurcation, when $\tau > \tau_N$, an attracting invariant circle appears.

In what follows, to obtain a more detailed dynamic behavior of the equilibrium point (u^*, v^*), we give the Neimark-Sacker bifurcation diagram in Figure 1, from which it is not difficult to find that when $\tau \in (0, \tau_N)$, (u^*, v^*) is stable. When $\tau > \tau_N$, stable invariant circles emerge. As τ continues to grow, there are some periodic orbits and phenomena like chaos.

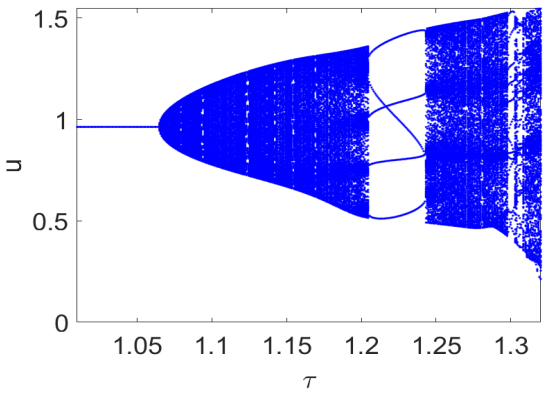

Figure 1. Diagram of Neimark-Sacker bifurcation

Next, from the Neimark-Sacker bifurcation diagram Figure 1, we use the phase portraits to illustrate the dynamic changes from stable focus, as τ increases. In particular, one has the stable focus at $\tau = 1.015$ in Figure 2(a). Increasing the value of τ to 1.065, as $\tau > \tau_N$, from Theorem 3.1 and Figure 1, we know that (u^*, v^*) loses stability and an attractive invariant circle bifurcates, as shown in Figure 2(b). When τ is equal to 1.21 and 1.3 respectively, the period window shown in Figure 1(a) is reached, period-5 and period-14 orbits emerge, as shown in Figure 2(c) and Figure 2(e) respectively. When $\tau = 1.256$, there exist quasi-periodic orbits in Figure 2(d). When τ finally hits 1.32, we get a chaotic attractor (see Figure 2(f)). From the above analysis, it is not difficult to obtain that with the increase of

τ, mapping (2.9) experiences dynamic changes from stable focus to invariant circle, through periodic window, and finally to the chaotic attractor.

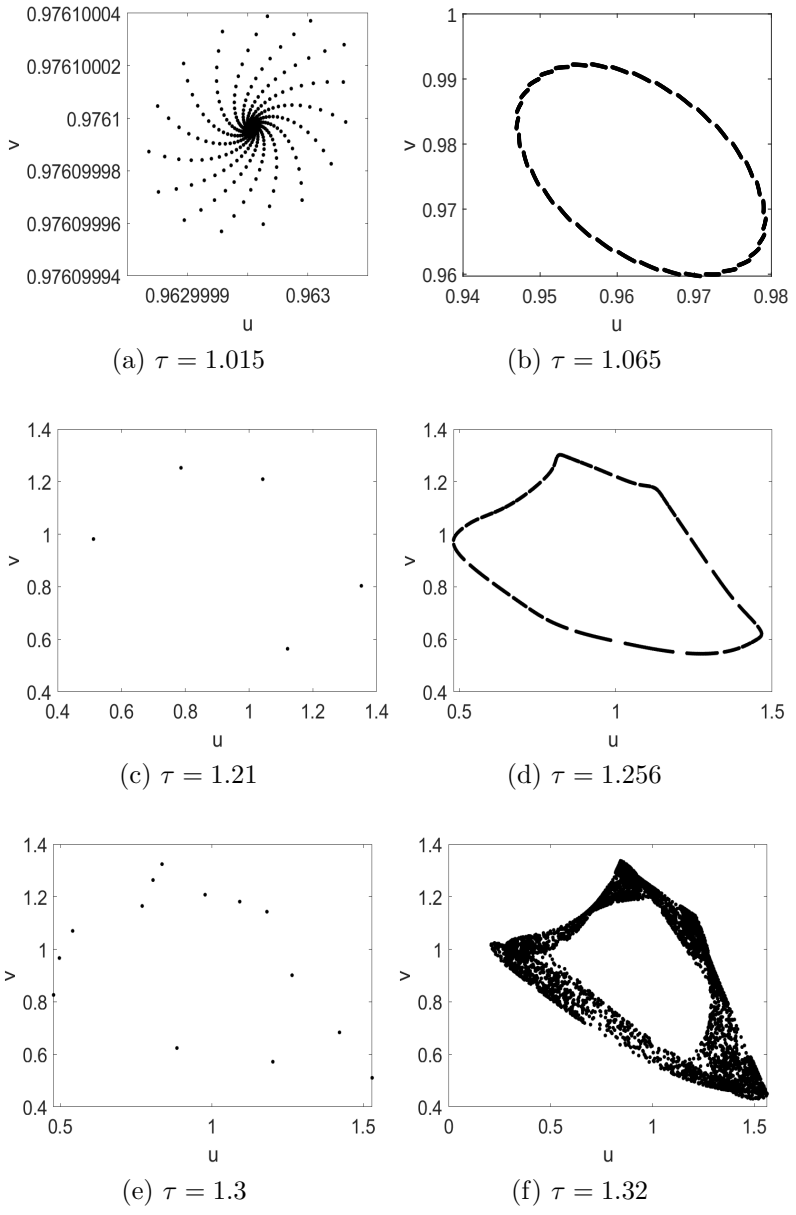

(a) $\tau = 1.015$ (b) $\tau = 1.065$

(c) $\tau = 1.21$ (d) $\tau = 1.256$

(e) $\tau = 1.3$ (f) $\tau = 1.32$

Figure 2. Phase portraits corresponding to different values τ in Figure 1

Moreover, we illustrate the spatial patterns on a 512×512 lattice with a spatial step $\delta = 5$. That is, $n = 512$. In Figure 3(a), we plot Z_m with respect to τ to obtain the Turing instability threshold. From Figure 3(a), we can observe that the critical value of Turing instability is $\tau_T = 1.066$. Also, in Figure 3(b), we have drawn the Neimark-Sacker and the Turing bifurcation curves respectively. It can be seen that

the parameter space is divided into four regions I-IV by $\tau = \tau_T$ and $\tau = \tau_N$. They are the homogeneous steady-state region, the Neimark-Sacker instability region, the Turing instability region and the Neimark-Sacker-Turing instability region. In region IV, Neimark-Sacker bifurcation and Turing instability appear, resulting in many complex patterns.

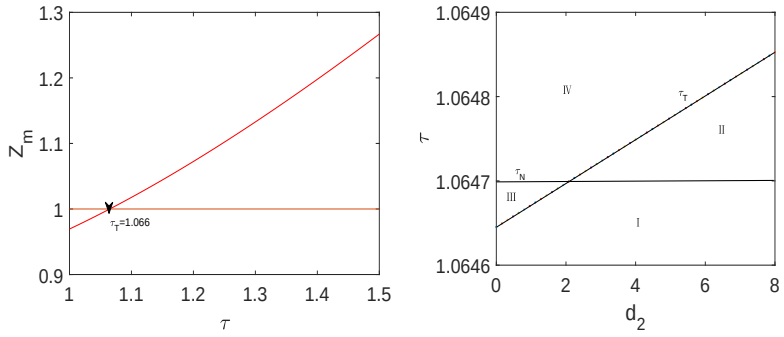

Figure 3. (a): $\tau - Z_m$ graph showing the Turing bifurcation; (b): $d_2 - \tau$ diagram showing pattern formation area

Under the condition that $d_1 = 1.5$, $d_2 = 4$ and $\delta = 5$, the spatial patterns are generated by Neimark-Sacker-Turing instability (see Figures 4 and 5). Let $\tau = 1.015$, neither Neimark-Sacker bifurcation nor Turing bifurcation will occur, then no spatial patterns are formed, as shown in Figure 4(a). When $\tau > \tau_T$, Neimark-Sacker-Turing instability occurs, leading to the formation of spatial heterogeneous patterns. For example, let $\tau = 1.065$, we get the spot pattern induced by the invariant circle (see Figure 4(b)). As the value of τ continues to increase, we can find curled and spiral patterns. For example, when τ is taken as $1.21, 1.256$ and 1.3 respectively, the patterns are shown in Figure 5(a)-(c) respectively. Compared with Figure 5(a), Figure 5(c) has a significantly greater curled. When τ finally increases to 1.32, the pattern becomes more fragmented, as shown in Figure 5(d).

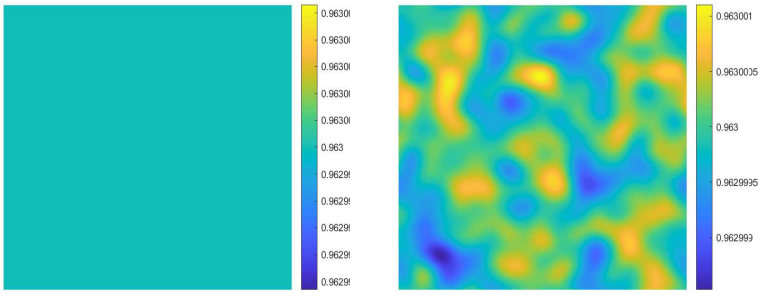

(a) $\tau = 1.015$ (b) $\tau = 1.065$

Figure 4. Spatial patterns induced by Neimark-Sacker-Turing instability

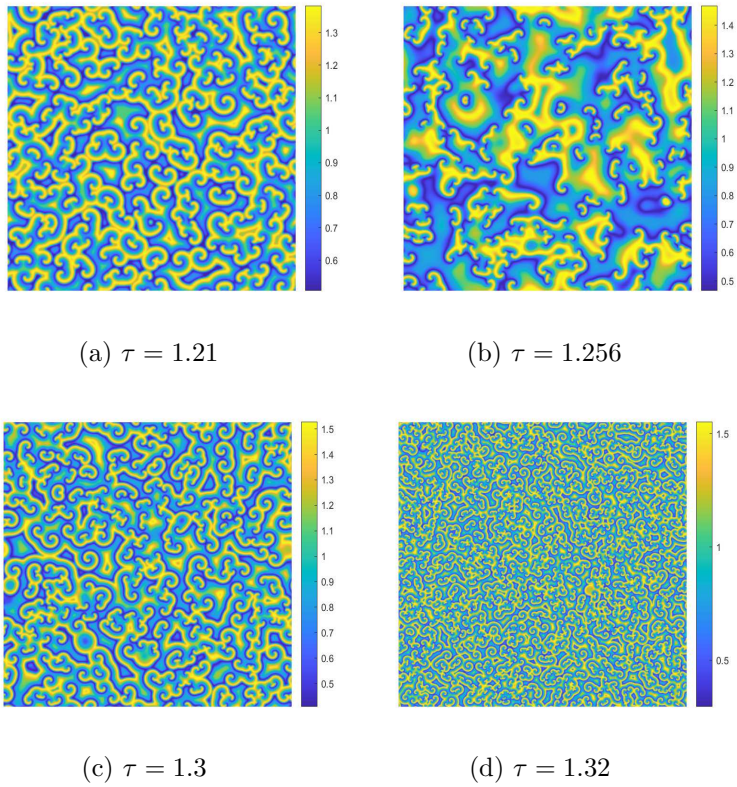

(a) $\tau = 1.21$ (b) $\tau = 1.256$

(c) $\tau = 1.3$ (d) $\tau = 1.32$

Figure 5. Continued

4.2. Flip bifurcation and related Turing patterns

Setting $a = 2.963$ and $b = 0.94$, then the equilibrium point is $(u^*, v^*) = (2.963, 0.3172)$. By direct calculation, it can be concluded that equation (3.10) and condition $(S41)$ in Theorem 3.2 are satisfied. The critical value of flip bifurcation is $\tau_F = 0.2598$. We take values in the neighborhood of τ_F, and get the following results.

When $\tau = 0.226$, the eigenvalues are $\lambda_1 = -0.74$ and $\lambda_2 = 0.7423$. Therefore, (u^*, v^*) is a stable node, which is consistent with Proposition 2.1. For $\tau = 0.2632 > \tau_F$, the eigenvalues are $\lambda_1 = -1.0264, \lambda_2 = 0.6999$, then (u^*, v^*) is unstable, and the stable period-2 points are $(2.774, 0.5013)$ and $(3.152, 0.1725)$, as shown in Figure 5(b). Letting $\tau = \tau_F$, then the eigenvalues are -1 and 0.7037, $\eta_1 = -7.7805 < 0, \eta_2 = 0.4673 > 0$.

According to Theorem 3.2, mapping (2.9) undergoes flip bifurcation at $\tau = \tau_F$. The bifurcation diagram of τ in the interval $[0.25, 0.31]$ is presented, as shown in Figure 6, from which the period-doubling sequence of activator concentration u can be clearly found. Clearly, when $\tau \in (0, \tau_F)$, there is a stable node. When τ is slightly larger than τ_F, (u^*, v^*) loses its stability, and there is a stable period-2 points. When τ continues to increase, periodic window and chaos appear.

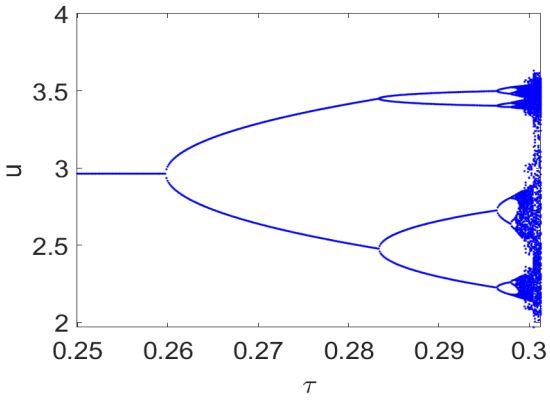

Figure 6. Diagram of flip bifurcation

To better illustrate these properties of the flip bifurcation, we give the phase portraits in Figures 7 and 8. Wherein Figure 7(a) corresponds to the stable equilibrium point at $\tau = 0.226$. Figure 7(b) is the period-2 at $\tau = 0.2632$. With increasing τ, we observe the doubling period. For example, if $\tau = 0.285$, the period-4 points are $(2.386, 0.9356)$, $(2.567, 0.7859)$, $(3.43, 0.05649)$, $(3.469, -0.002621)$, as shown in Figure 8(a). When the value of τ is properly increased, the period will be further doubled. For example, if $\tau = 0.2966$, there is a stable periodic-8 orbit, as shown in Figure 8(b). Finally, the chaotic attractor at $\tau = 0.2992$ is shown in Figure 8(c).

For more detailed information about chaotic attractor, we give a local magnifications of Figure 8(c) (see Figure 8(d)). It can be found from Figures 7 and 8 that with different τ values, the dynamic changes from stable equilibrium point to chaotic paths as illustrated in flip bifurcation diagram.

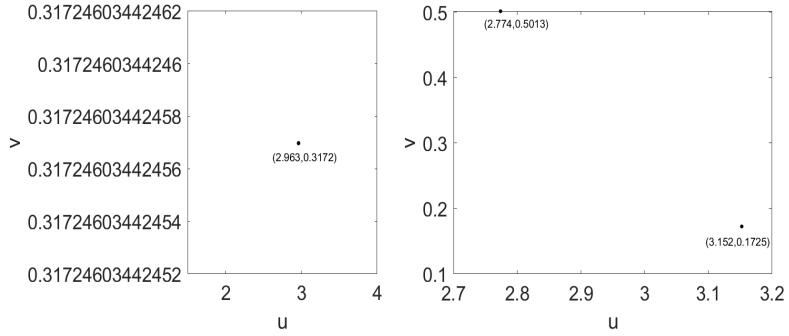

(a) $\tau = 0.226$ (b) $\tau = 0.2632$

Figure 7. Phase portraits for different value τ corresponding to Figure 6

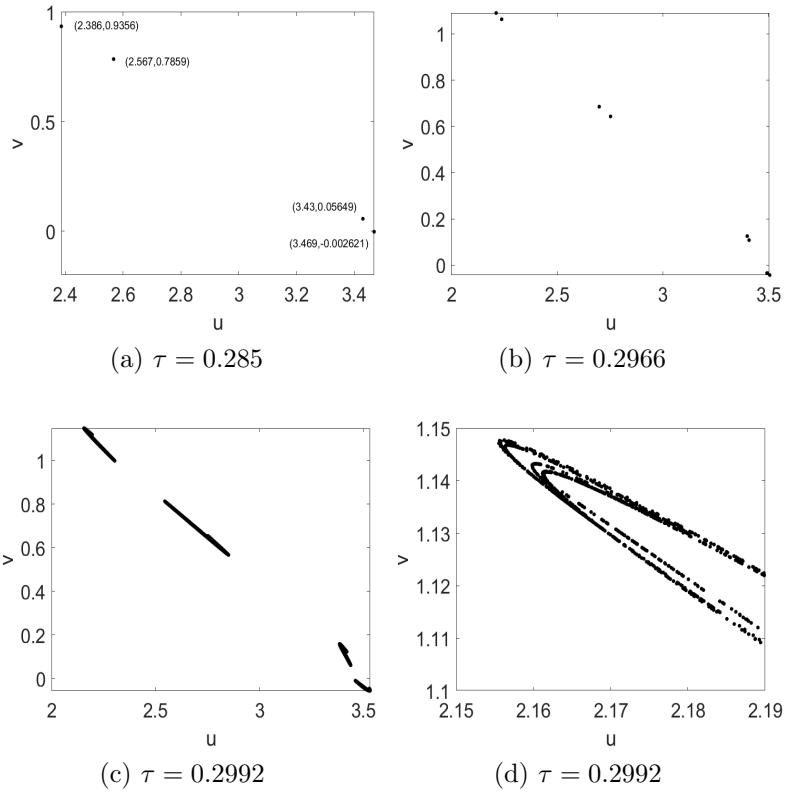

(a) $\tau = 0.285$ (b) $\tau = 0.2966$

(c) $\tau = 0.2992$ (d) $\tau = 0.2992$

Figure 8. Continued

Supposing $d_1 = 1.5, d_2 = 4.5$, $\delta = 5$ and $n = 512$, we plot the variation of Z_m with respect to τ to determine the Turing bifurcation threshold value τ_T in Figure 9(a). It can be seen that the critical value of Turing instability $\tau_T = 0.2578$. In Figure 9(b), the curves of the flip bifurcation and Turing bifurcation are respectively drawn. Note that these two curves divide the parameter space into three regions I-III. They are the homogeneous steady-state region, the Turing instability region and the flip-Turing instability region respectively. In region III, the flip bifurcation and Turing instability appear, resulting in many complex patterns.

Furthermore, in Figure 10, we simulate the spatial patterns of the activator concentration u caused by the flip-Turing instability and chaos mechanism corresponding to Figures 7 and 8. The initial state is a random disturbance of uniform steady state (u^*, v^*). We assume $\tau = 0.226$, neither flip bifurcation nor Turing bifurcation will occur, then no spatial pattern is formed, as shown in Figure 10(a). When τ is greater than τ_T, flip-Turing instability will occur, leading to the generation of spatial heterogeneous patterns. For example, letting $\tau = 0.2632$, $\tau = 0.278$ and $\tau = 0.285$, the patterns are shown in Figure 10(b)-(d) respectively. As τ increases to 0.2966, the pattern caused by period-8 orbits is shown in Figure 10(e). When τ reaches 0.2992, the pattern induced by chaos attractor becomes more disordered and irregular, as shown in Figure 10(f).

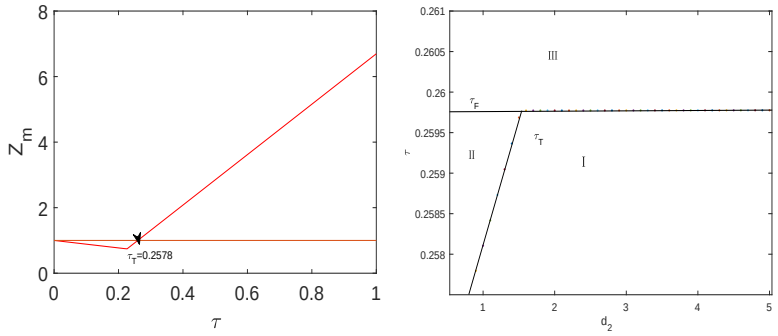

(a) (b)

Figure 9. (a): $\tau - Z_m$ graph showing the Turing bifurcation; (b): $d_2 - \tau$ diagram showing pattern formation area

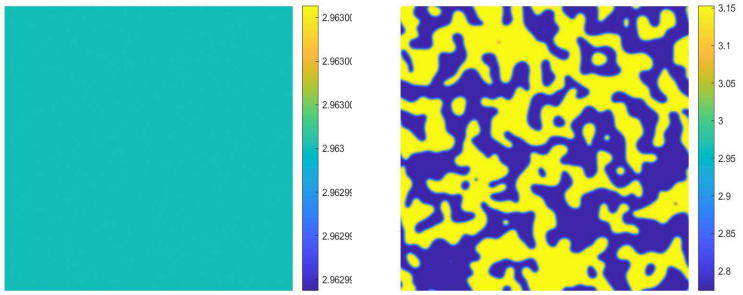

(a) $\tau = 0.226$ (b) $\tau = 0.2632$

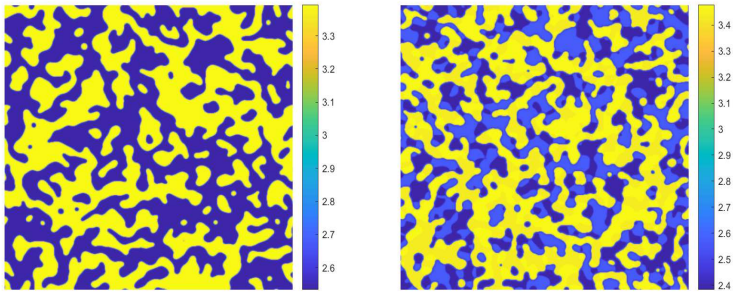

(c) $\tau = 0.278$ (d) $\tau = 0.285$

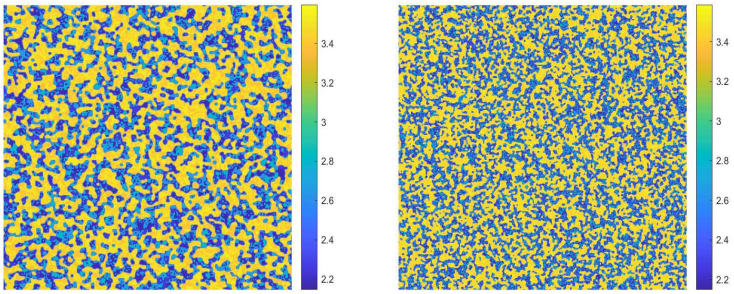

(e) $\tau = 0.2966$ (f) $\tau = 0.2992$

Figure 10. Spatial patterns induced by flip-Turing instability

Remark 4.1. Through the theoretical analysis and numerical simulations, we can see that discrete Brusselator model could undergo Neimark-Sacker bifurcation, flip bifurcation and producing patterns that are either circles, curly or spirals, and eventually chaos. However, for the continuous Brusselator system, in [16], Hopf bifurcation analysis and the stability of periodic solutions were discussed. Global bifurcation was discussed in [4]. In [30], the Turing stability of the positive constant steady state was studied and the amplitude equations near the Turing-Hopf codimension-2 point were derived. The more interesting and complex dynamical behaviors will be found for the discrete and continuous Brussselator models.

5. Conclusions

The spatiotemporal dynamics of the Brusselator model with discrete time and discrete space are considered. Compared with the existing results about system (2.2), the CML model established in this paper has some more interesting dynamical behaviors. The coupled mapping lattice method is applied to the continuous Brusselator system to obtain the discrete system, which is different from the previous discrete versions. Then, through theoretical analysis, the parametric conditions for the stable homogeneous stationary state, flip bifurcation, Neimark-Sacker bifurcation and Turing instability are given respectively. Finally, numerical simulations are performed to verify the theoretical analysis, and abundant spatial patterns, such as periodic windows, invariant circles and chaos, are obtained. These behaviors are induced through the combination of Neimark-Sacker bifurcation and flip bifurcation with Turing instability. Various patterns are found in the numerical simulation. Moreover, the effects of parameter τ on the patterns are also manifested. It can be found that when the parameter τ increases, the spatiotemporal pattern changes from regular to irregular, and finally to disorder. Patterns, for example, begin to curl and gradually break into pieces. These changes may reflect the interaction between the activator and the inhibitor.

Acknowledgments

We are very grateful to the reviewers and editors for their valuable suggestions, which have helped improve our paper.

References

[1] W. Abid, R. Yafia, M. A. Aziz-Alaoui, H. Bouhafa and A. Abichou, *Diffusion driven instability and Hopf bifurcation in spatial predator-prey model on a circular domain*, Applied Mathematics and Computation, 2015, 260, 292–313.

[2] L. Bai and G. Zhang, *Nontrivial solutions for a nonlinear discrete elliptic equation with periodic boundary conditions*, Applied Mathematics and Computation, 2009, 210(2), 321–333.

[3] P. Baydemir, H. Merdan, E. Karaoglu and G. Sucu, *Complex Dynamics of a Discrete-Time Prey-Predator System with Leslie Type: Stability, Bifurcation Analyses and Chaos*, International Journal of Bifurcation and Chaos, 2020, 30(10), Article ID 2050149, 21 pages.

[4] K. J. Brown and F. A. Davidson, *Global bifurcation in the Brusselator system*, Nonlinear Analysis: Theory, Methods & Applications, 1995, 24(12), 1713–1725.

[5] L. Chang, G. Sun, Z. Wang and Z. Jin, *Rich dynamics in a spatial predator–prey model with delay*, Applied Mathematics and Computation, 2015, 256, 540–550.

[6] Q. Din, *A novel chaos control strategy for discrete-time Brusselator models*, Journal of Mathematical Chemistry, 2018, 56, 3045–3075.

[7] X. Fu, R. Wu, M. Chen and H. Liu, *Spatiotemporal complexity in a diffusive Brusselator model*, Journal of Mathematical Chemistry, 2021, 59, 2344–2367.

[8] W. Gao and B. Dai, *Dynamics of a Predator-prey Model with Delay and Fear Effect*, Journal of Nonlinear Modeling and Analysis, 2019, 1(1), 57–72.

[9] A. A. Golovin, B. J. Matkowsky and V. A Volpert, *Turing Pattern Formation in the Brusselator Model with Superdiffusion*, SIAM Journal on Applied Mathematics, 2008, 69(1), 251–272.

[10] J. Guckenheimer and P. Holmes, *Nonlinear Oscillations, Dynamical Systems, and Bifurcations of Vector Fields*, Springer-Verlag, New York, 1983.

[11] G. Guo, J. Wu and X. Ren, *Hopf bifurcation in general Brusselator system with diffusion*, Applied Mathematics and Mechanics (English Edition), 2011, 32(9), 1177–1186.

[12] Z. Guo, H. Huo, Q. Ren and H. Xiang, *Bifurcation of a Modified Leslie-Gower System with Discrete and Distributed Delays*, Journal of Nonlinear Modeling and Analysis, 2019, 1(1), 73–91.

[13] T. Huang, H. Yang, H. Zhang, X. Cong and G. Pan, *Diverse self-organized patterns and complex pattern transitions in a discrete ratio-dependent predator–prey system*, Applied Mathematics and Computation, 2018, 326, 141–158.

[14] T. Huang and H. Zhang, *Bifurcation, chaos and pattern formation in a space and time-discrete predator–prey system*, Chaos, Solitons & Fractals, 2016, 91, 92–107.

[15] Y. Jia, Y. Li and J. Wu, *Coexistence of activator and inhibitor for Brusselator diffusion system in chemical or biochemical reactions*, Applied Mathematics Letters, 2016, 53, 33–38.

[16] B. Li and M. Wang, *Diffusion-driven instability and Hopf bifurcation in Brusselator system*, Applied Mathematics and Mechanics (English Edition), 2008, 29(6), 825–832.

[17] Y. Li, *Oscillation deduced from the Neimark-Sacker bifurcation in a discrete dual Internet congestion control algorithm*, Advances in Difference Equations, 2013, 136, 11 pages.

[18] M. Liao and Q. Wang, *Stability and Bifurcation Analysis in a Diffusive Brusselator-Type System*, International Journal of Bifurcation and Chaos, 2016, 26(7), Article ID 1650119, 11 pages.

[19] M. Ma and J. Hu, *Bifurcation and stability analysis of steady states to a Brusselator model*, Applied Mathematics and Computation, 2014, 236, 580–592.

[20] D. C. Mistro, L. A. D. Rodrigues and S. Petrovskii, *Spatiotemporal complexity of biological invasion in a space- and time discrete predator–prey system with the strong Allee effect*, Ecological Complexity, 2012, 9, 16–32.

[21] A. H. Nayfeh and B. Balachandran, *Applied Nonlinear Dynamics: Analytical, Computational, and Experimetal Methods*, Wiley-VCH Verlag GmbH, Co. KGaA, Weinheim, 1995.

[22] J. Neimark, *On Some Cases of Periodic Motion Depending on Parameters*, Doklady Akademii Nauk SSSR, 1959, 129, 36–39.

[23] I. Prigogene and R. Lefever, *Symmetry Breaking Instabilities in Dissipative Systems. II*, Journal of Chemical Physics, 1968, 48(4), 1665–1700.

[24] D. Punithan, D. K. Kim and R. I. Mckay, *Spatiotemporal dynamics and quantification of daisyworld in two-dimensional coupled map lattices*, Ecological Complexity, 2012, 12, 43–57.

[25] P. C. Rech, *Nonlinear Dynamics of Two Discrete-Time Versions of the Continuous-Time Brusselator Model*, International Journal of Bifurcation and Chaos, 2019, 29(10), Article ID 1950142, 7 pages.

[26] L. A. D. Rodrigues, D. C. Mistro and S. Petrovskii, *Pattern formation in a space- and time-discrete predator–prey system with a strong Allee effect*, Theoretical Ecology, 2012, 5, 341–362.

[27] R. S. Sacker, *On invariant surfaces and bifurcations of periodic solutions of ordinary differential equations*, Journal of Difference Equations and Applications, 2009, 15(8–9), 759-774.

[28] A. Singh and P. Deolia, *Bifurcation and Chaos in Predator–Prey Model with Holling Type-III Functional Response and Harvesting Effect*, Journal of Biological Systems, 2021, 29(2), 451–478.

[29] A. M. Turing, *The Chemical Basis of Morphogenesis*, Philosophical Transactions of the Royal Society of London. Series B. Biological Sciences, 1952, 237, 37–72.

[30] J. C. Tzou, Y. P. Ma, A. Bayliss, B. J. Matkowsky and V. A. Volpert, *Homoclinic snaking near a codimension-two Turing-Hopf bifurcation point in the Brusselator model*, Physical Review E, 2013, 87, Article ID 022908, 20 pages.

[31] J. Wang, Y. Li, S. Zhong and X. Hou, *Analysis of bifurcation, chaos and pattern formation in a discrete time and space Gierer Meinhardt system*, Chaos, Solitons & Fractals, 2019, 118, 1–17.

[32] S. Wiggins, *Introduction to Applied Nonlinear Dynamical Systems and Chaos*, Springer-Verlag, New York, 1991.

[33] F. Zhang, H. Zhang, T. Huang, T. Meng and S. Ma, *Coupled Effects of Turing and Neimark-Sacker Bifurcations on Vegetation Pattern Self-Organization in a Discrete Vegetation-Sand Model*, Entropy, 2017, 19(478), 991–1004.

[34] H. Zhang, X. Cong, T. Huang, S. Ma and G. Pan, *Neimark-Sacker-Turing Instability and Pattern Formation in a Spatiotemporal Discrete Predator-Prey System with Allee Effect*, Discrete Dynamics in Nature and Society, 2018, Article ID 8713651, 18 pages.

[35] S. Zhong, J. Wang, J. Bao, Y. Li and N. Jiang, *Spatiotemporal Complexity Analysis for a Space-Time Discrete Generalized Toxic-Phytoplankton-Zooplankton Model with Self-Diffusion and Cross-Diffusion*, International Journal of Bifurcation and Chaos, 2021, 31(1), Article ID 2150006, 27 pages.